nature ecology & evolution

SUPPLEMENTARY INFORMATION

https://doi.org/10.1038/s41559-020-1136-3

In the format provided by the authors and unedited.

A ^{14}C chronology for the Middle to Upper Palaeolithic transition at Bacho Kiro Cave, Bulgaria

Helen Fewlass[1]✉, Sahra Talamo[1,2], Lukas Wacker[3], Bernd Kromer[1,4], Thibaut Tuna[5], Yoann Fagault[5], Edouard Bard[5], Shannon P. McPherron[1], Vera Aldeias[1,6], Raquel Maria[1], Naomi L. Martisius[7], Lindsay Paskulin[8], Zeljko Rezek[1,9], Virginie Sinet-Mathiot[1], Svoboda Sirakova[10], Geoffrey M. Smith[1], Rosen Spasov[11], Frido Welker[1,12], Nikolay Sirakov[10], Tsenka Tsanova[1] and Jean-Jacques Hublin[1,13]

[1]Department of Human Evolution, Max Planck Institute for Evolutionary Anthropology, Leipzig, Germany. [2]Department of Chemistry 'G. Ciamician', University of Bologna, Bologna, Italy. [3]Ion Beam Physics, ETH Zürich, Zürich, Switzerland. [4]Institute of Environmental Physics, University of Heidelberg, Heidelberg, Germany. [5]CEREGE, Aix-Marseille University, CNRS, IRD, INRA, Collège de France, Aix-en-Provence, France. [6]ICArEHB, University of Algarve, Campus de Gambelas, Faro, Portugal. [7]Department of Anthropology, University of California, Davis, CA, USA. [8]Department of Archaeology, University of Aberdeen, Aberdeen, UK. [9]University of Pennsylvania Museum of Archaeology and Anthropology, Philadelphia, PA, USA. [10]National Institute of Archaeology and Museum, Bulgarian Academy of Sciences, Sofia, Bulgaria. [11]Archaeology Department, New Bulgarian University, Sofia, Bulgaria. [12]Evolutionary Genomics Section, Globe Institute, University of Copenhagen, Copenhagen, Denmark. [13]Collège de France, Paris, France.
✉e-mail: helen_fewlass@eva.mpg.de

Supplementary Information

A ^{14}C chronology for the Middle–to–Upper Palaeolithic transition at Bacho Kiro Cave, Bulgaria

Helen Fewlass[1]*, Sahra Talamo[1,2], Lukas Wacker[3], Bernd Kromer[1,4], Thibaut Tuna[5], Yoann Fagault[5], Edouard Bard[5], Shannon P. McPherron[1], Vera Aldeias[6,1], Raquel Maria[1], Naomi L. Martisius[7], Lindsay Paskulin[8], Zeljko Rezek[1,9], Virginie Sinet-Mathiot[1], Svoboda Sirakova[10], Geoffrey M. Smith[1], Rosen Spasov[11], Frido Welker[12,1], Nikolay Sirakov[10], Tsenka Tsanova[1], Jean-Jacques Hublin[1,13]

1) Department of Human Evolution, Max Planck Institute for Evolutionary Anthropology, Leipzig, Germany
2) Department of Chemistry "G. Ciamician", University of Bologna, Bologna, Italy
3) Ion Beam Physics, ETH Zürich , Zürich, Switzerland
4) Institute of Environmental Physics, University of Heidelberg, Heidelberg, Germany
5) CEREGE, Aix-Marseille University, CNRS, IRD, INRA, Collège de France, Aix-en-Provence, France
6) ICArEHB, University of Algarve, Campus de Gambelas, Faro, Portugal
7) Department of Anthropology, University of California, Davis, USA
8) Department of Archaeology, University of Aberdeen, Aberdeen, Scotland
9) University of Pennsylvania Museum of Archaeology and Anthropology, Philadelphia, PA, USA
10) National Institute of Archaeology and Museum, Bulgarian Academy of Sciences, Sofia, Bulgaria
11) Archaeology Department, New Bulgarian University, Sofia, Bulgaria
12) Evolutionary Genomics Section, Globe Institute, University of Copenhagen, Copenhagen, Denmark
13) Collège de France, Paris, France

* **Corresponding author:** helen_fewlass@eva.mpg.de

Supplementary Text

1. Stratigraphy and site formation

Bacho Kiro Cave consists of a deep labyrinthine karst system extending 3,600 m[1] through Cretaceous sandy limestones and sandstones, with evidence of human occupation near the cave's entrance. The current entrance is ~4 m wide and connects in the SW to the inner karst system. The bottom Pleistocene deposits (Layers K, J, and I) consist of sand, silt and clay originating from siliciclastic accumulations present inside the karst system and interstratified with common angular limestone debris (gravel-size and larger) resulting from local spalling of the cave's roof and walls. The cave's floor morphology dips towards the cave's entrance, and hence these lower Pleistocene layers are thicker near the entrance and eventually pinch out towards its interior. Therefore, as one approaches the south part of the cave in the Main Sector, Layer K is absent and Layers J and I eventually disappear, with only the upper (more recent) part of Layer J being present along grid rows F-G and eventually also abutting against bedrock (Fig. 1c). Layers K, J and I are, thus, better represented in the Niche 1 area (Fig. 1d). Here, Layer N1-K rests directly on bedrock and is loamy sands showing some lateral variability in terms of the frequency of limestone clasts (normally in the 3-8 cm range and rarer large clasts up to 15 cm at the top of the Layer N1-K), and varies from reddish brown in the SE to lighter brown towards the NW. It contains rare domains (diameter of max 10 cm) of darker sediments with small (<1 cm width) charcoal fragments. These seem to be remnants of poorly preserved combustion features. Towards its top, there is a marked increase in weathered limestones, which may point to some weathering of the surface of N1-K deposits. The contact between Layer N1-K and the overlying N1-J is, however, overall gradual, possibly due to a slow rate of deposition. Layer N1-J is a greenish brown loamy clay, ~20 cm thick and pinching out against the bedrock towards the south. It has frequent limestone clasts, typically around 5 cm in diameter, but also a few larger angular limestone clasts up to 20 cm wide, attesting to local contribution of roof fall, with a relative increase of small limestone clasts and granules towards its top. The contact with the above Layer N1-I is sharp and clear in Niche 1 where Layer N1-I is a particularly distinctive dark brown sticky loamy clay that thins out towards the cave walls (5-8 cm thick in the eastern profile of Niche 1). In the Main Sector, Layer I is thinner and consists of dark brown sandy clays with common limestone rubbles (typically in the 4-10 cm range and occasional dm-sized blocks). In both the field and in thin section, there are abundant charcoals and bones (some burned), including evidence of trampling (in-situ broken bones). These characteristics point to a relative depositional stasis with an increase of anthropogenic inputs, including abundant accumulation of combustion and occupational debris. The frequency of archaeological material and the reduced thickness of this layer show that human occupants were basically living on top of debris from previous occupations, pointing to a slower sedimentation rate. Despite some lateral variability and the fact that we are at the spatial limit of the extension of Layer I in the Main Sector, combined stratigraphic, sedimentary and archaeological content make the correlation between Layers N1-I and I clear.

Layers I/N1-I have a sharp, erosive contact with the overlying Layers G and N1-H/G. In the Main Sector this contact is associated with dm-sized limestone blocks. Layers G and N1-H/G are well-laminated silts and sands that mark a shift in the sedimentation mechanisms at the site, with rapid accumulation from runoff by a low-energy stream originating from inside the karst system. Layer N1-H should be

seen as a subdivision of Layer N1-G present only in the Niche 1 sequence. Under thin section, the alternating and bedded nature of silts and fine sands are evident, including clay-rich lenses, small (few µm in size) rounded carnivore coprolites and clay papules. The very rare archaeological artefacts (bone fragments) are in the lowermost contact and are reworked, ripped up material from the surface of Layer I.

Layers F, E and D in the Main Sector and Layers N1-3e, N1-3d and N1-3c in the Niche 1 are sub-horizontal deposits composed of fine silts and clays with some sand, varying from increased clay content (grey lenses) to silty sands (orange lenses) with rare stones in the Niche 1 and few limestones clasts (typically 7-10 cm) in the Main Sector. Sedimentary sources relate mainly to reworking of fine siliciclastic deposits from inside the cave system and point to relatively rapid deposition rates. The top of these deposits is truncated and associated with partial erosion towards the south (in Niche 1) and southeast (in the Main Sector), indicating the presence of a sedimentary outlet and the continuation of the cave's chamber (albeit probably small-sized opening) into the south-southeast. Layers N1-3b and C are thus stratigraphic markers in both excavation areas, showing a change in sedimentary dynamics with preferential accumulation of coarser rubble from local spalling of the cave roof and walls. The above Layers B and A are preserved in the Main Sector and seem to relate to formation processes like those described for Layers F-D. These are fine sediments, with few stones and varying from darker brown lenses intercalated with orange brown silty clays. As with Layers F-D, stratigraphic contacts are often diffuse and show an undulating morphology pointing to plastic alteration of the deposits occurring post-depositionally. Such folding is particularly visible in the convoluted morphology of the rare, discrete charcoal-rich combustion features present in Layers B and A (see Fig. 1c). The uppermost section of Layer A (A0) corresponds to the current surface of the cave floor cut by previous excavations and incorporating recent materials.

2. Collagen extraction and quality control methods

Bone collagen was extracted in the Department of Human Evolution at the MPI-EVA, Leipzig, following the protocol described in Fewlass et al[2]. Briefly, the outer surface of the bone was removed with a sand blaster and samples were removed with a Dremel drill. Bones were demineralised in HCl 0.5M until soft and CO_2 effervescence had stopped. Samples were treated with NaOH 0.1M to remove humic acid contamination and re-acidified in HCl 0.5M. The samples were gelatinised in weakly acidic water (HCl pH3) based on the method described by Longin[3]. Soluble collagen samples were passed through a pre-cleaned Ezee filter (Elkay labs, UK) and pre-cleaned ultrafilter (Sartorius Vivaspin Turbo 15) to concentrate the large molecular weight fraction (>30 kD) for AMS dating[4-6]. Background-level bones (older than 50,000 BP) kindly supplied by D. Döppes (Mannheim, Germany) were extracted alongside the samples in order to assess contamination introduced in the laboratory.

Approximately 0.5 mg collagen from each extract was weighed into a tin cup and measured on a ThermoFinnigan Flash elemental analyser (EA) coupled to a Thermo Delta plus XP isotope ratio mass spectrometer (IRMS) to determine their stable isotopic ($\delta^{13}C$ and $\delta^{15}N$) and elemental values (C%, N%, C:N). Stable carbon isotope ratios were expressed relative to VPDB (Vienna PeeDee Belemnite) and stable nitrogen isotope ratios were measured relative to AIR (atmospheric N_2) using the delta notation

(δ) in parts per thousand (‰). Repeated analysis of internal and international standards indicates an analytical error of 0.2‰ (1σ) for $\delta^{13}C$ and $\delta^{15}N$.

A small aliquot of each collagen sample (*ca.* 300 µg) was homogenised in an agate mortar and pestle, then mixed with ~40 mg of IR grade KBr powder, pressed into a pellet using a manual hydraulic press (Wasserman) and analysed with an Agilent Technologies Cary 660 Fourier transform infra-red (FTIR) spectrometer (Agilent Technologies, Santa Clara) with a deuterated triglycine sulfate (DTGS) detector. Spectra were recorded in transmission mode at 4 cm^{-1} resolution and averaging of 34 scans between 4000 and 400 cm^{-1} using Resolution Pro software (Agilent Technologies, Santa Clara). The obtained spectra were evaluated and compared to library spectra of well-preserved collagen and bone.

3. ZooMS collagen fingerprinting methods

All 147 bone specimens that were pretreated in the radiocarbon study were also analysed though MALDI-TOF-MS collagen peptide mass fingerprinting (ZooMS)[7,8]. A small bone sample (<20 mg) was taken from each bone or dentine specimen independent of the radiocarbon sample. An ammonium-bicarbonate buffer extraction was performed, including digestion with trypsin (0.5 µg/µL, Promega), pH acidification using TFA (20% TFA) and cleaning on C18 ZipTips (Sigma-Aldrich/Thermo Scientific). Digested peptides were analysed on a MALDI-TOF-MS using previously published protocols[9]. MALDI-TOF-MS spectra were compared to a reference database containing collagen peptide marker masses of all medium to larger sized genera in existence in western Eurasia during the Late Pleistocene[9].

4. Comparison of degradation measured through collagen extraction for radiocarbon dating and ZooMS analysis

For each ZooMS spectrum, the extent of deamidation was assessed for two peptides containing a single glutamine (peptides P1105 and P1706)[10-12]. This allows us to assess the existence of any formal relationship between the different measures of collagen/proteome degradation used in either radiocarbon dating or ZooMS. For radiocarbon dating, we took the frequently reported values of the collagen % and C:N ratio as indicators of collagen preservation. For ZooMS, we took the number of observed peptide markers and P1105 and P1706 deamidation as indicators of collagen preservation.

Independently, measures of preservation show tight clustering in areas that, for each measure, are indicative of well-preserved proteins (Supplementary Fig. 5). For example, most ZooMS spectra contain nine observable peptide markers (out of nine possible). We observe no obvious correlations where higher rates of deamidation are linked to samples with more divergent C:N ratios or lower collagen % (Supplementary Fig. 5c, d, e, f). The only suggestion of such a correlation might be for the number of peptide markers, as ZooMS spectra with less than four observable peptide markers also result in collagen percentage below 5% (Supplementary Fig. 5b). In addition, specimens without any peptide markers present also have extremely low, or no, collagen yields after extraction for radiocarbon dating. This does not hold for all specimens, as there are also bone specimens with the majority of peptide markers present but that also have low collagen yields (<0.5%). From the Bacho Kiro Cave dataset, we therefore conclude that ZooMS spectral quality and/or glutamine deamidation

measures in ZooMS spectra is a poor predictor for the successful extraction of collagen for radiocarbon dating.

5. Faunal composition of the ^{14}C dataset

ZooMS analysis shows that the faunal sample set includes a large amount of *Ursidae*, *Bos/Bison*, *Equidae*, *Cervid/Saiga* and *Capra sp.* and two bones of *Rhinoceratidae* (Supplementary Table 2), fully in agreement with the zooarchaeological interpretation of the whole faunal collection[8]. Signs of human modification are present (63% of the dated bones across all layers) on bones of all represented species, except the two *Rhinoceratidae* bones. Whereas 16.5% of the faunal collection from Layer N1-I/I shows signs of human modification, only 1.8% has traces of carnivore modification (tooth marks, signs of gnawing or digestion), indicating that human agency played a large role in the composition of the faunal assemblage in the IUP layers in the cave[8]. Many of the *Ursidae* remains (Cave bear/Brown bear), both in the overall dataset and in the ^{14}C dataset, bear traces of human modification, including perforated teeth and butchery marks indicative of skinning. The evidence suggests close interactions between the humans occupying the cave and bears, with humans either scavenging dead animals for furs, bone and teeth, or hunting them due to competition for food or shelter[13,14]. Ongoing zooarchaeological analyses will help more clearly define this relationship alongside other human subsistence behaviours at Bacho Kiro Cave.

6. Outlier analysis of dates

Fourteen dates out of the 67 included in the outlier analysis were identified as outliers based on their posterior outlier probabilities, agreement index and depositional histories (shown in red in supplementary Table 4)[15,16]. The three dates from the uppermost Layer A1 are wide-ranging. The layer contains the youngest-dated bone in the sequence at 23,130 ± 60 ^{14}C BP (ETH-86796) which is over 7,000 years younger than any other obtained date from the site. No micromorphological factor has so far been identified to be responsible for the wide range of dates in this layer. However, since the reason for such a wide range of dates is currently unknown all three dates were excluded from the modelling.

One date from Layer B (ETH-71299) was slightly younger than the other dates from the layer and was identified as an outlier. This date is statistically identical to the date (ETH-86768) of the hominin bone BK-1751 from the 1970s collection which was labelled as layer 6a/7 (B/C). The inclusion of the hominin bone in the model may have affected the posterior outlier probability of ETH-71299, but as the exact stratigraphic context of this hominin bone is unknown it was not included and we excluded ETH-71299 as an outlier.

ETH-71303 (41,720 ± 180 ^{14}C BP) is much older than the other dates within Layer C, but we have no explanation for this outlier. It was excluded from further analysis.

ETH-71307 (36,500 ± 110 ^{14}C BP) is younger than the other dates in Layer E. As this bone was excavated from close to the contact zone of Layers E and D the prior probability was set to 1.0 in the outlier analysis, and it was also excluded from the modelling.

Micromorphological analysis indicates that Layer G consists of water deposited sediment and the artefacts within it were re-deposited from the underlying Layer I by water moving through the cave. The radiocarbon dates support this interpretation so the prior probabilities of these dates were set to 1.0 during outlier analysis, and the five dates from Layer G and N1-G were excluded from modelling. Two of the youngest dates from Layer I (ETH-86779; ETH-86782) were identified as outliers based on their agreement index and posterior outlier probabilities. One date from the upper part of Layer J (ETH-93193) was inconsistent with its stratigraphic position with a posterior outlier probability of 1.0. These three dates were also excluded.

When the remaining 53 dates from the Main Sector and Niche 1 are modelled (Fig. 3; Supplementary Table 5) the agreement indices of both models are well above 60%, indicating that none of the dates included need to be rejected[16]. Due to the archaeological and micromorphological links between Layer I and N1-I in the Main Sector and Niche 1, we combined the dates from the two areas into one Bayesian model (Supplementary Fig. 6). When we ran this combined model, the agreement index was very low (A_{model}=28.9) with six dates having lower agreement indices and/or a higher posterior outlier probability than when the areas are modelled separately (Supplementary Table 4). We consider this to be a reflection of the different spatial accumulation of Layer J in the two locations and the much larger number of dates from N1-I in the Niche 1, rather than the AMS measurements or context of these bones being erroneous. We therefore consider the two individual models (Fig. 3) as the most accurate reflection of the stratigraphy in the cave.

Supplementary Figures

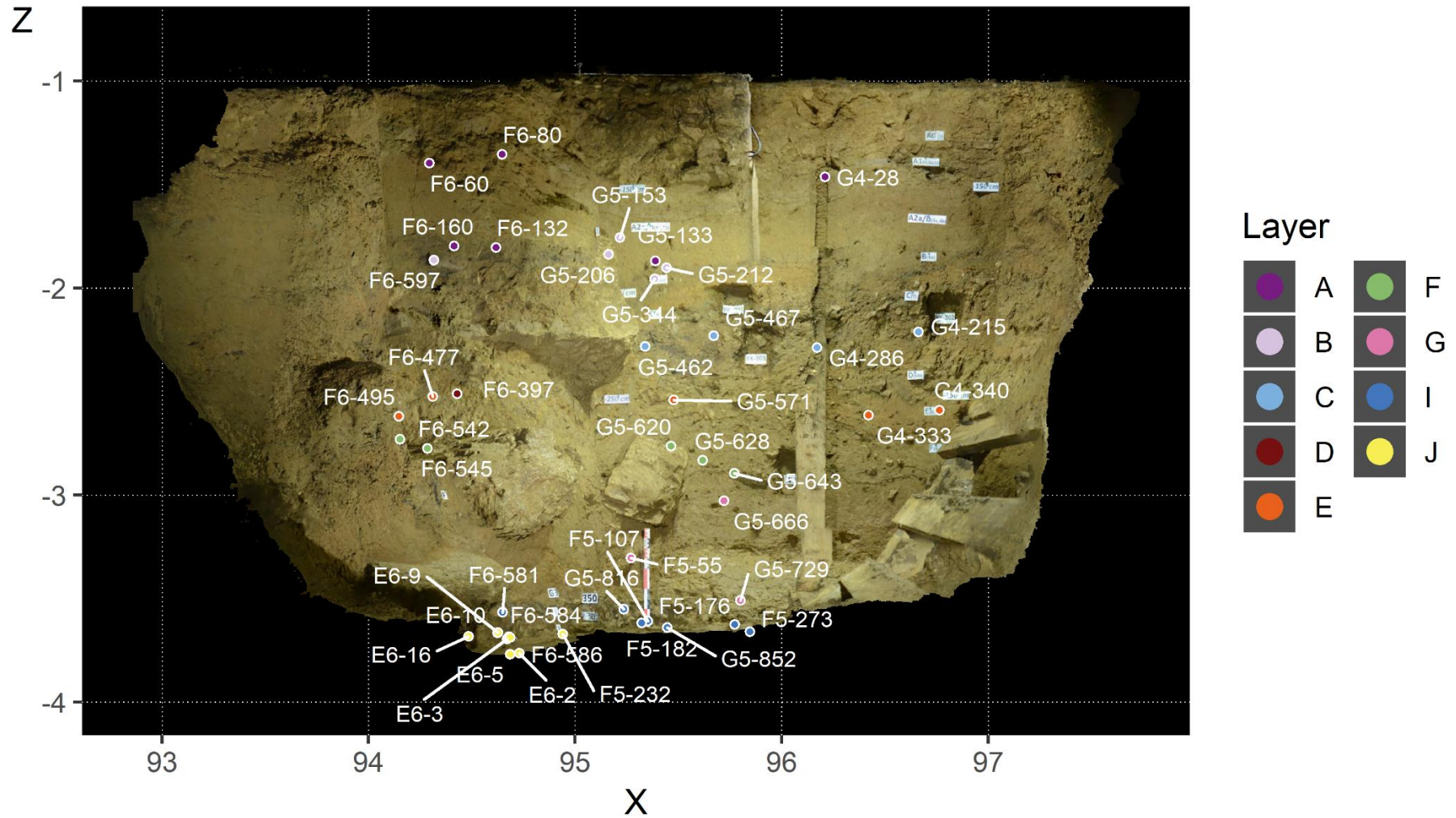

Supplementary Figure 1. 3D model of the transversal stratigraphic profile in the Main Sector (facing north-east) showing the location of all the bones dated in the study marked with their square ID (corresponding to Supplementary Table 2) according to layer. 3D models produced in AgiSoft PhotoScan.

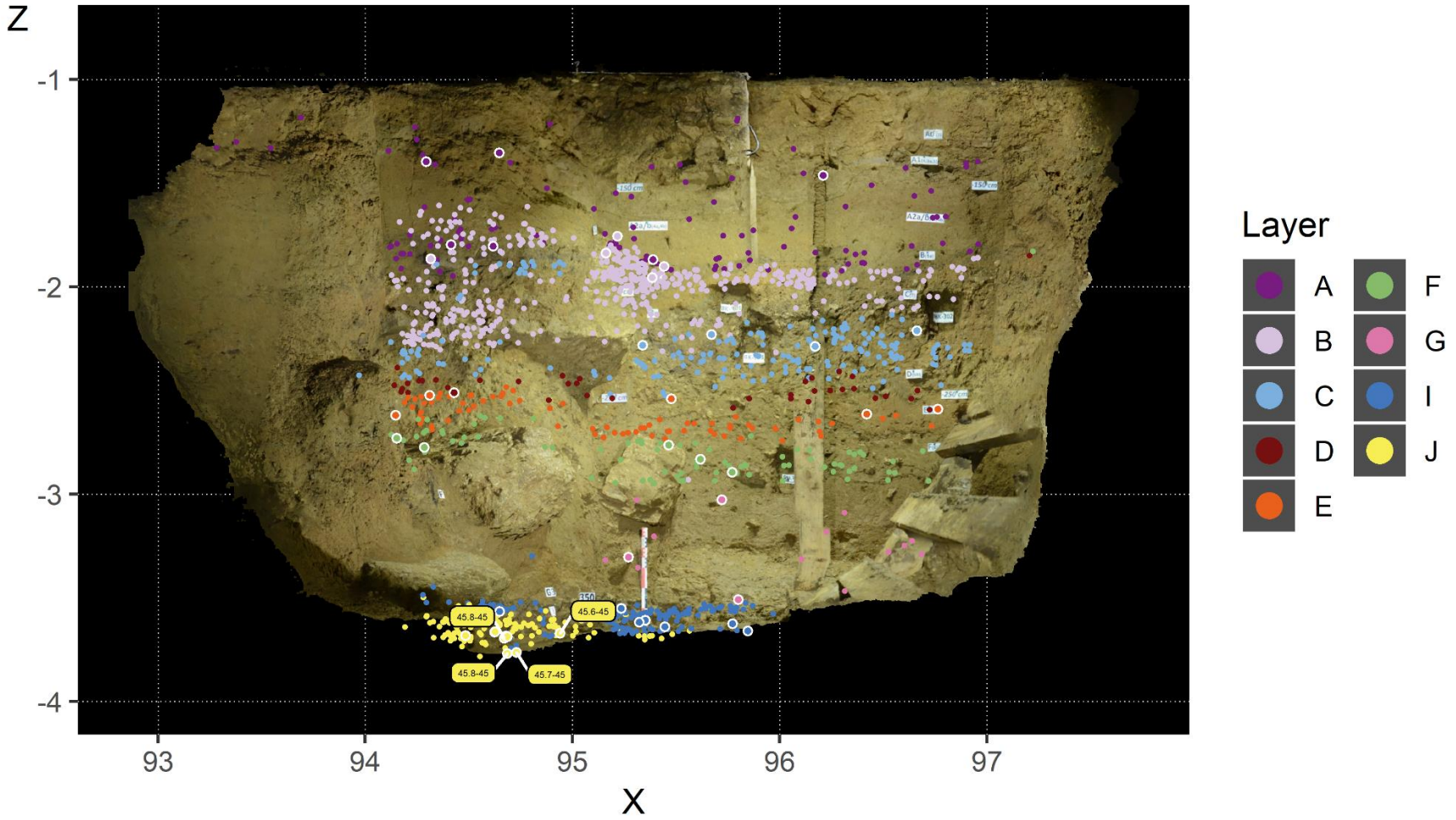

Supplementary Figure 2. 3D model of the transversal stratigraphic profile in the Main Sector (facing north-east) showing all the finds separated by layer excavated during 2015-2018. The bones dated in the study are marked with a white circle. Select radiocarbon dates are shown (ka BP; 95% calibrated range). Note the variable density of finds between layers.

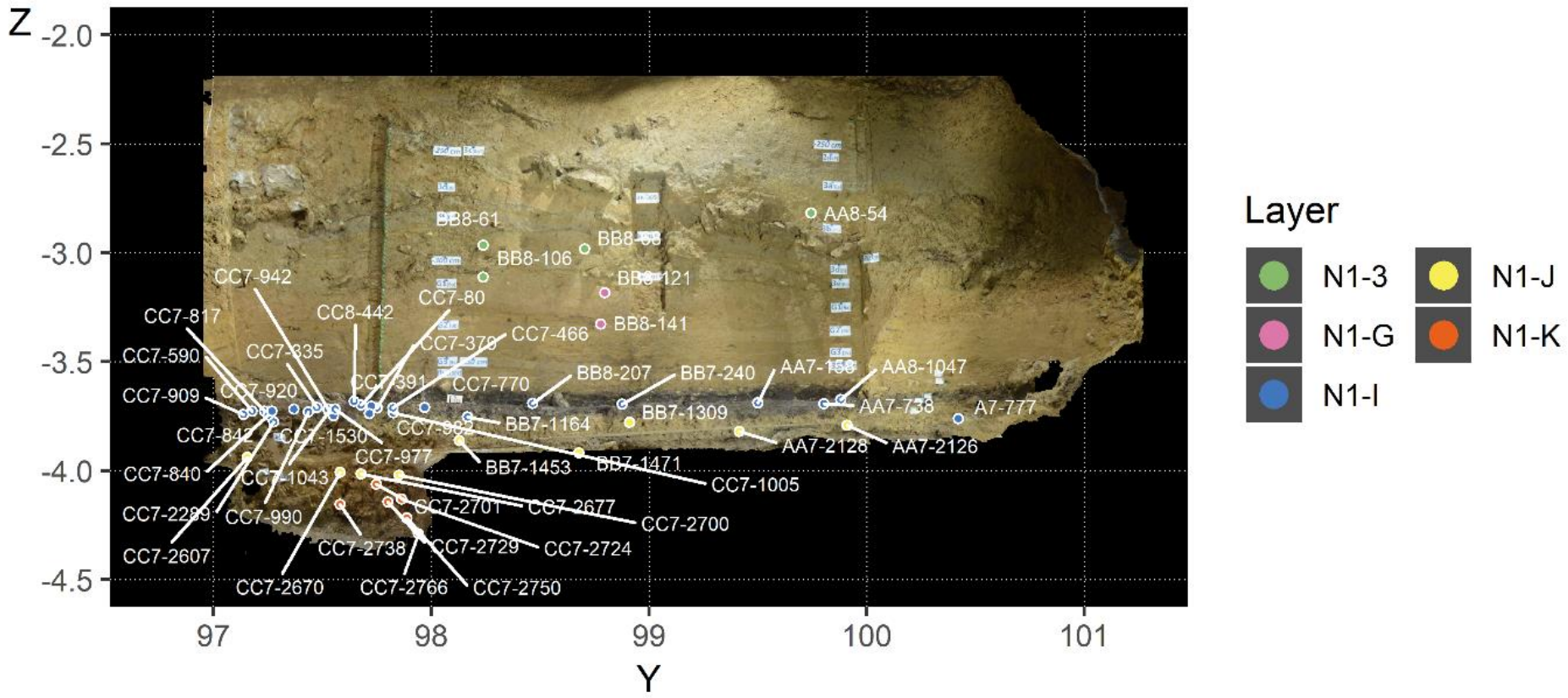

Supplementary Figure 3. 3D model of the longitudinal stratigraphic profile in the Niche 1 (facing north-west) showing the location of all the bones dated in the study marked with their square ID (corresponding to Supplementary Table 2) separated according to layer.

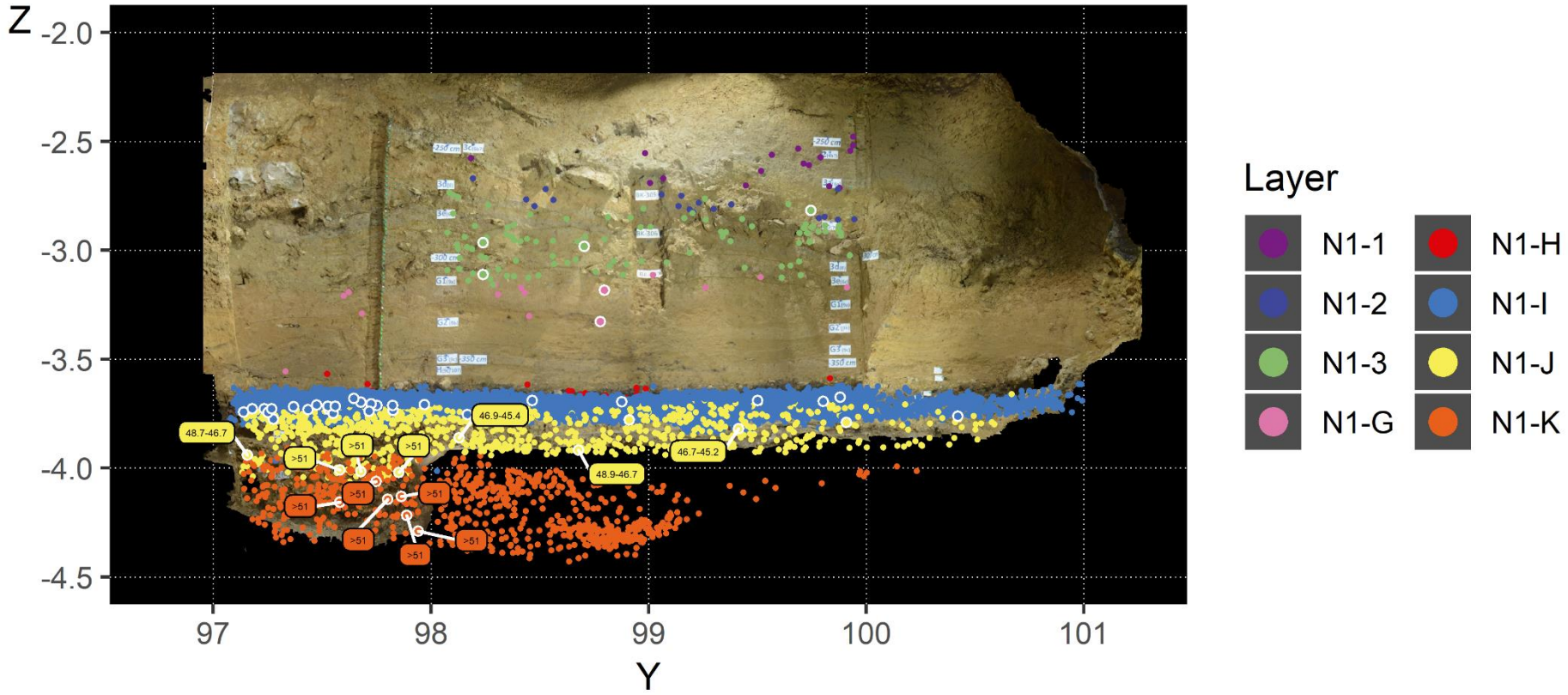

Supplementary Figure 4. 3D model of the longitudinal stratigraphic profile in the Niche 1 (facing north-west) showing all the finds separated by layer excavated during 2015-2019. The bones dated in the study are marked with a white circle. Select radiocarbon dates are shown (ka BP; 95% calibrated range). Note that the density of finds is exceptionally high in Layer N1-I.

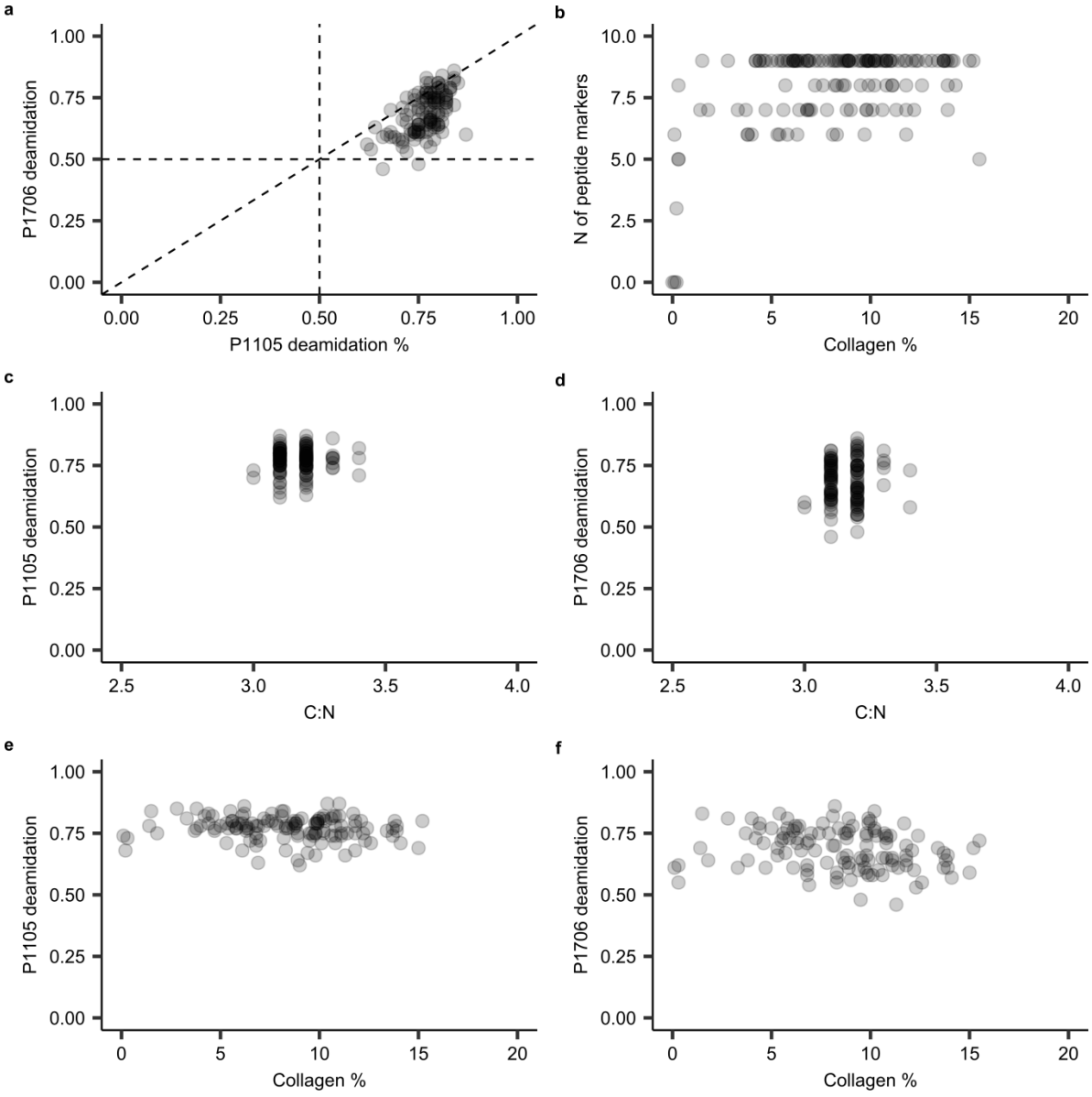

Supplementary Figure 5. Relationship between collagen preservation (^{14}C data) and glutamine deamidation (ZooMS data): **a)** Correlation between collagen peptide P1105 and P1706 deamidation; **b)** Relationship between the collagen % and number of observed peptide markers; **c)** Relationship between the C:N ratio and P1105 deamidation; **d)** Relationship between the C:N ratio and P1706 deamidation; **e)** Relationship between collagen % and P1105 deamidation; **f)** Relationship between collagen % and P1706 deamidation. For deamidation, 1 indicates no deamidation and 0 indicates complete deamidation of the single glutamine in either the P1105 or P1706 peptide.

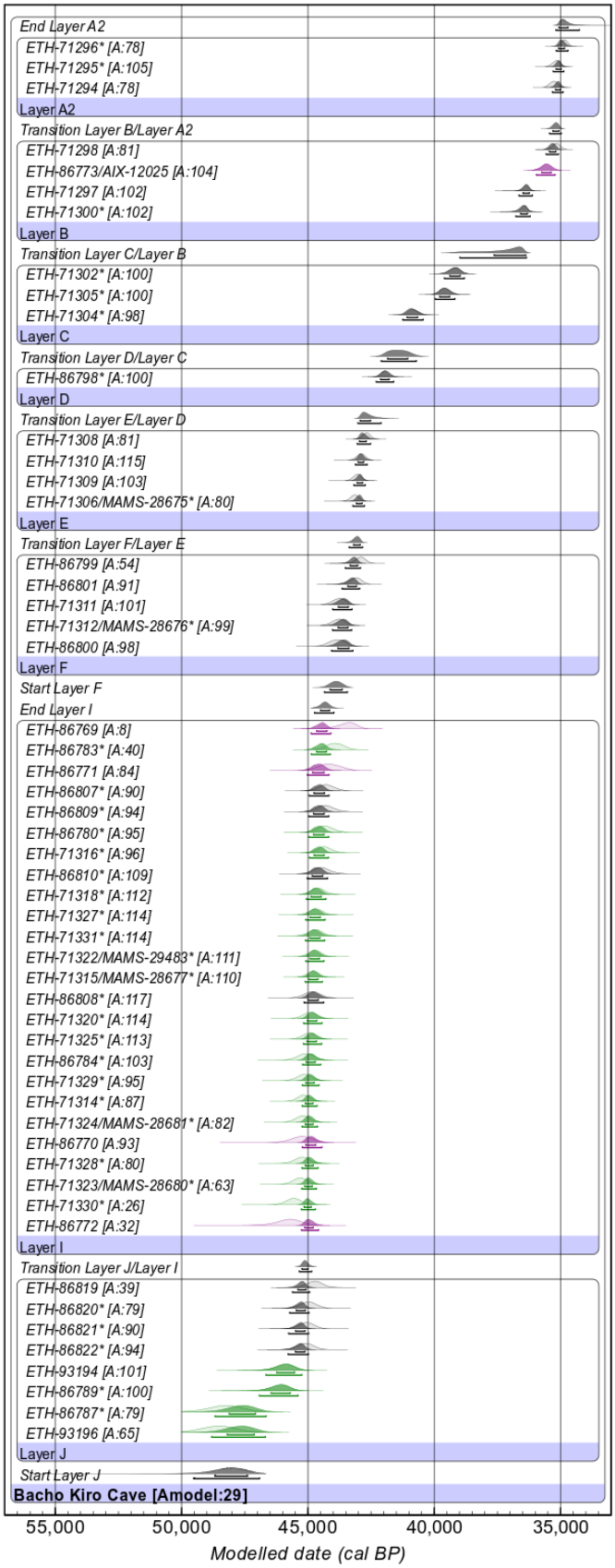

Supplementary Figure 6. Bayesian chronological model for Bacho Kiro Cave on material excavated during the 2015-2017 field seasons from both the Main Sector and Niche 1 (model 3; Supplementary Table 5). The AMS lab numbers are shown on the left side. The dates were calibrated against the IntCal13 dataset[17], and the modelling was performed in OxCal 4.3[15]. Where more than one measurement was made from the same collagen extract, dates were combined (R_Combine) in OxCal 4.3. **The distributions of dates from the Niche 1 are shown in green and from the Main Sector in black. The dates from the hominin bones from Layer N1-I and Layer B are shown in purple.** The radiocarbon likelihoods of calibrated dates (without modelling) are shown in the lighter shade and the posterior distributions (after modelling) are darkly shaded. Brackets show the 68.2% and 95.4% probability ranges of the calibrated dates. Dates marked with an asterisk (*) are from bones bearing signs of anthropogenic modification.

This model includes all dates shown in Fig. 3, which have high levels of agreement when modelled within each area. The agreement index of this combined model (A_{model}=29) is below the generally accepted limit of 60%. The different depositional histories of Layer J in the two areas is reflected in the radiocarbon data. Note that two dates from the bottom of Layer N1-J are >51,000 BP (beyond model range) as are two dates from the N1-J/K contact and five dates from the underlying Layer N1-K. Further information is included in Supplementary Tables 2, 4, 5.

Supplementary Tables

Supplementary Table 1. Cultural identification of the stone assemblages from each layer of Bacho Kiro Cave, showing the correlation of the layers from the excavation in the 1970s[18] and the new excavation (2015-2018)[8].

Layer			Summary of techno-typological assemblages
Niche 1 (N1)	**Main Sector (MS)**	**1971-75 excavations**	
N1-1?	A1	4? 3a? 5?	• 2015-2018 – Main Sector: very low density (n=6) of Upper Palaeolithic forms including 2 backed bladelets, characteristic of the Gravettian. • 1970s – Very poor lithic assemblage named 'backed piece tradition' interpreted as Epigravettian.
N1-2?	A2	4a? 4b?	• 2015-2018 – Main Sector: low density of Upper Palaeolithic forms (n=12) without diagnostic tool types. • 1970s - 194 lithics interpreted as 'Aurignacian-like', including many flakes, a few blades and tools such as end-scrapers, burins, denticulate flakes and side-scrapers.
N1-3a?	B	6a?	• 2015-2018 – Main Sector: Upper Palaeolithic assemblage (n=87) with Aurignacian elements (bladelet cores with carenoidal end-scrapers, burins, retouched blades and engraved bone). • 1970s – Upper Palaeolithic assemblage (n=521) present only at the border with the underlying Layer 7. Assemblage described as typical Balkan Aurignacian (carenoidal and nosed end-scrapers, dihedral burins and spalls, retouched blades, thin backed bladelets with fine or step retouch).
N1-3b	C	7	• 2015-2018 – Main Sector: low density Upper Palaeolithic artefact assemblage (n=13): retouched blades, burin-core (*burin busqué*), worked bone and platforms consistent with the appearance of soft hammer percussion. • 1970s – Also attributed to the Aurignacian (lithics n=652): tools with typical Aurignacian retouch and typology, burins and bladelet cores.
N1-3c	D	6b?	• 2015-2018 – One lithic recovered in the Niche 1. • 1970s – Low density (n=74) present only at border with overlying layer 7: many flakes and a few blades, cores and tools (end-scrapers, burins and retouched blades).
N1-3d	E	8?	• 2015-2018 – No lithics recovered. • 1970s – 2 lithics.
N1-3e	F	6c?	• 2015-2018 – No lithics recovered.

			• 1970s – 1 lithic and 5 bone retouchers (and 4 bones with cut-marks).
N1-G	G	9c -9a	• 2015-2018 – Main Sector: Very low density (n=3) of lithics reworked from Layer I (water-laid deposit). No lithics in the Niche 1. • 1970s – Lithics (n=239) fitting with the technology and typology of the underlying Bachokirian assemblage. Aurignacian elements (retouched blades, high end-scrapers, bone points) gradually increase in Layers 9-7.
N1-H	Not present	9c/10	• 2015-2018 – Niche 1: low density of lithics (n=73) reworked from underlying layer N1-I (water-laid deposit). From the contact zone of Layer N1-H/I artefacts (n=129) are consistent with the lithics from Layer N1-I. • 1970s – No lithics in Layer 10.
N1-I	I	11	• 2015-2018 – High-density IUP assemblage (n=1395) consistent with 1970s excavation, made on various imported fine-grained flints, consisting of Levallois-like blades, retouched blade points, end-scrapers and splintered pieces. Assemblage is very fragmented and reworked. Also includes worked bone tools (awls, lissoirs, retouchers) and pendants (bear/ungulate teeth). • 1970s – Assemblage called 'Bachokirian Upper Palaeolithic' made on fine-grained imported flint. 19,834 lithics excavated from 58 m² (85 % are chips and tiny fragments < 15 mm). Tool types: end-scrapers, retouched blades and flakes, splintered pieces and burins.
N1-J	J	11a	• 2015-2018 – Low density (n=25) of lithics with distribution in keeping with previous excavation. In the lower part of Layer N1-J, 6 lithics are consistent with the overlying IUP and 8 consistent with the underlying Middle Palaeolithic from Layer N1-K. Relatively high number of lithics (n=41) in the contact zone of Layers N1-I/J, consistent with overlying IUP in Layer N1-I. • 1970s – In total, 51 lithics excavated. Upper part contains assemblage consistent with overlying Layer 11 but at much lower density. Lower portion of Layer 11a contains some Middle Palaeolithic artefacts consistent with Layer 12. Change from volcanic rock to flint at border of Layers 12/11a.
N1-K	Not present	12	• 2015-2018 – Middle Palaeolithic assemblage (n=82) consistent with 1970s excavation containing Levallois flakes. Raw material is local coarse-grained syenite porphyry. • 1970s – Middle Palaeolithic (Mousterian: Levallois flakes, bone retouchers) on local volcanic rock extends from Layer 14 to bottom of Layer 11a.

Not present	Not present	13	• 1970s – Relatively rich assemblage of Middle Palaeolithic (Mousterian) artefacts (n=786).
Not present	Not present	14	• 1970s – Low number of Middle Palaeolithic (Mousterian) lithics (n=5).

Supplementary Table 2. Sample information of all bones from Bacho Kiro Cave extracted in the radiocarbon study (*sheet 1 in accompanying .xlsx file*).

Supplementary Table 3. AMS measurements of bone collagen backgrounds (>50,000 BP) and instrumental backgrounds (*sheet 2 in accompanying .xlsx file*).

Supplementary Table 4. Comparison of outlier analysis and agreement index of three Bayesian models from Bacho Kiro Cave (*sheet 3 in accompanying .xlsx file*).

Supplementary Table 5. Comparison of Bayesian model output for Bacho Kiro Cave chronology (outliers excluded) (*sheet 4 in accompanying .xlsx file*).

Supplementary Table 6. Comparison of radiocarbon dates of the two Upper Palaeolithic human bone fragments, BK-1653 and F6-597, using 2.5-3 mg collagen in graphite targets measured with the MICADAS at ETH Zürich, and using 100-300 µg collagen for the gas ion source of the AixMICADAS[19,2]. The bottom line shows the weighted mean ^{14}C age and 1σ error of all the dates from each extract, calculated using the R_Combine function in OxCal 4.3[15]. The output of the X^2 test is included in the bottom line showing that all the dates are statistically indistinguishable for the two bones (for the dates to be in statistical agreement the T value must be less than the X^2 value which is shown in parentheses). All dates have been rounded to the nearest 10 years.

	BK-1653						**F6-597**					
Dating method	**AMS Lab no**	**µg C**	**F^{14}C**	**error**	**^{14}C age (BP)**	**1 σ error**	**AMS Lab no**	**µg C**	**F^{14}C**	**error**	**^{14}C age (BP)**	**1σ error**
Graphite	ETH-86768	996	0.0223	0.0004	30540	140	ETH-86773	940	0.0197	0.0004	31540	150
CO_2	AIX-12024.1.1	48	0.0229	0.0015	30330	530	AIX-12025.1.1	84	0.0189	0.0013	31880	570
CO_2	AIX-12024.1.2	36	0.0218	0.0013	30720	490	AIX-12025.1.2	68	0.0187	0.0014	31960	600
CO_2	AIX-12024.1.3	39	0.0214	0.0013	30870	490	AIX-12025.1.3	90	0.0177	0.0011	32400	490
CO_2	AIX-12024.1.4	93	0.0221	0.0011	30610	400						
R_Combine	df = 4, T= 0.8 (5% 9.5)				30570	120	df = 3, T= 3.5 (5% 7.8)				31660	140

References

1 Briestenský, M. *et al.* Evidence of a plate-wide tectonic pressure pulse provided by extensometric monitoring in the Balkan Mountains (Bulgaria). *Geologica Carpathica* **66**, 427-438 (2015).

2 Fewlass, H. *et al.* Pretreatment and gaseous radiocarbon dating of 40–100 mg archaeological bone. *Scientific Reports* **9**, 5342, doi:10.1038/s41598-019-41557-8 (2019).

3 Longin, R. New method of collagen extraction for radiocarbon dating. *Nature* **231**, 241-242 (1971).

4 Brown, T. A., Nelson, D. E., Vogel, J. S. & Southon, J. R. Improved collagen extraction by modified Longin method. *Radiocarbon* **30**, 171-177 (1988).

5 Bronk Ramsey, C., Higham, T., Bowles, A. & Hedges, R. Improvements to the pretreatment of bone at Oxford. *Radiocarbon* **46**, 155-164 (2004).

6 Brock, F., Bronk Ramsey, C. & Higham, T. Quality assurance of ultrafiltered bone dating. *Radiocarbon* **49**, 187–192 (2007).

7 Buckley, M., Collins, M., Thomas-Oates, J. & Wilson, J. C. Species identification by analysis of bone collagen using matrix-assisted laser desorption/ionisation time-of-flight mass spectrometry. *Rapid Communications in Mass Spectrometry* **23**, 3843-3854, doi:10.1002/rcm.4316 (2009).

8 Hublin, J.-J. *et al.* Initial Upper Palaeolithic *Homo sapiens* remains from Bacho Kiro Cave (Bulgaria). *Nature,* doi:10.1038/s41586-020-2259-z (2020).

9 Welker, F. *et al.* Palaeoproteomic evidence identifies archaic hominins associated with the Châtelperronian at the Grotte du Renne. *Proceedings of the National Academy of Sciences* **113**, 11162 (2016).

10 Wilson, J., van Doorn, N. L. & Collins, M. J. Assessing the extent of bone degradation using glutamine deamidation in collagen. *Analytical Chemistry* **84**, 9041-9048, doi:10.1021/ac301333t (2012).

11 Doorn, N. L., Wilson, J., Hollund, H., Soressi, M. & Collins, M. J. Site-specific deamidation of glutamine: a new marker of bone collagen deterioration. *Rapid Communications in Mass Spectrometry* **26**, 2319-2327, doi:10.1002/rcm.6351 (2012).

12 Welker, F. *et al.* Variations in glutamine deamidation for a Châtelperronian bone assemblage as measured by peptide mass fingerprinting of collagen. *STAR: Science & Technology of Archaeological Research* **3**, 15-27, doi:10.1080/20548923.2016.1258825 (2017).

13 Romandini, M. *et al.* Bears and humans, a Neanderthal tale. Reconstructing uncommon behaviors from zooarchaeological evidence in southern Europe. *Journal of Archaeological Science* **90**, 71-91, doi:10.1016/j.jas.2017.12.004 (2018).

14 Terlato, G. *et al.* Chronological and isotopic data support a revision for the timing of cave bear extinction in Mediterranean Europe. *Historical Biology*, 1-11, doi:10.1080/08912963.2018.1448395 (2018).

15 Bronk Ramsey, C. Bayesian analysis of radiocarbon dates. *Radiocarbon* **51**, 337-360 (2009).

16 Bronk Ramsey, C. Dealing with outliers and offsets in radiocarbon dating. *Radiocarbon* **51**, 1023-1045 (2009).

17 Reimer, P. J. *et al.* IntCal13 and Marine13 radiocarbon age calibration curves 0–50,000 years cal BP. *Radiocarbon* **55**, 1869–1887 (2013).

18 Kozłowski, J. K. *Excavation in the Bacho Kiro cave (Bulgaria): Final Report*. (Państwowe Wydawnictwo Naukowe, 1982).

19 Bard, E. *et al.* AixMICADAS, the accelerator mass spectrometer dedicated to ^{14}C recently installed in Aix-en-Provence, France. *Nuclear Instruments and Methods in Physics Research Section B: Beam Interactions with Materials and Atoms* **361**, 80-86, doi:10.1016/j.nimb.2015.01.075 (2015).